Sensors and Materials, Vol. 38, No. 4 (2026) 1817–1827
MYU Tokyo

S & M 4408

Characterization of Optical Properties in Vanadium Dioxide Thin Films through Semiconductor-to-metal Transition

Amal M. Al-Amri[1*] and Waad S. Alharbi[2]

[1]Physics Department, College of Science & Arts King Abdulaziz University, Rabigh 25724,Saudi Arabia
[2]Department of Chemistry, College of Science University of Jeddah, Jeddah 23738, Saudi Arabia

(Received January 5, 2026; accepted March 5, 2026)

Keywords: vanadium dioxide thin films, optical properties of VO_2, phase transition in VO_2, smart windows technology, photonic and optoelectronic applications

Vanadium dioxide (VO_2) is a phase-change material between the monoclinic (M) and rutile (R) phases of the lattice with an insulator-to-metal transition (IMT) at 68 ˚C. This transition offers massive modifications in its optical properties, such as the refractive index, extinction coefficient, reflectance, and transmittance. These features make VO_2 highly attractive to the smart window technology, as it enables the utilization of solar heat and transparency under dynamic control to maximize energy savings. In this study, VO_2 thin films were modeled to investigate the phase-controlled optical characteristics of such materials in terms of the refractive index (n), the extinction coefficient (k), and the transmittance. The coefficients were determined using the dielectric function to assess the light behavior in each phase. The transmittance was also considered to depend on the film thickness. The results showed that the metallic phase has a higher reflectance and lower transmittance than the semiconducting phase. It was observed that there was a minor increase in transmittance with increasing thickness, and hence, film geometry can be applied in fine-tuning the optical performance. Such findings can be used to design the VO_2-based devices to optimize them, particularly with regard to smart windows, among other photonic uses.

1. Introduction

Vanadium dioxide (VO_2) is a strongly correlated electron system that undergoes a sharp first-order insulator-to-metal transition (IMT) at ~341 K (68 ℃).(1) This thermally reversible transition can also be triggered by electric fields, optical excitation, or mechanical stress, and is accompanied by dramatic changes in electrical, optical, thermal, and mechanical properties.(2) The IMT is associated with a rearrangement of the electron band structure accompanied by a carrier concentration change of up to four orders of magnitude, depending on the character of the Mott-type electron correlation and Peierls structure distortion.(3) At elevated temperatures, VO_2 adopts a metallic rutile (R) structure with tetragonal symmetry (space group P42/mNm). When cooled, it transitions into the monoclinic (M1) phase (space group P21/c), becoming an

*Corresponding author: e-mail: amsalamri@kau.edu.sa
https://doi.org/10.18494/SAM6154

ISSN 0914-4935
https://myukk.org/

insulator with a bandgap of approximately 0.6 eV. The M1 phase is characterized by a zigzag pairing (dimerization) of vanadium ions along the rutile c-axis, which gives it semiconducting properties. This dimerization is lost when VO_2 reverts to the metallic rutile phase at higher temperatures, resulting in enhanced infrared reflectivity and elevated thermal emissivity. [4,5]

The dramatic difference in these phases renders VO_2 an excellent candidate in photonic and optoelectronic applications as optical switches, thermally tunable emitters and nonlinear devices. Critically, the optical properties of VO_2 thin films are susceptible to such factors as thickness, epitaxial strain, crystallographic symmetry, grain structure, and impurity concentration. This can have a direct influence on the refractive index (n), extinction coefficient (k), transmittance (T), and reflectance (R), and can therefore be used to tune the performance accurately.[6] In addition to optics, the IMT also causes changes in resistivity of several orders of magnitude, reflecting the multifunctional character of VO_2.[7]

Smart windows are one of the more interesting applications. With such windows, solar heat flux and optical transmission can be regulated dynamically by controlling the thermochromic transition of VO_2 to minimize building energy consumption.[8] Correlations between VO_2 thin-film thickness and optical behavior, together with substrate-dependent effects, were established in previous studies.[9–12] Nevertheless, systematic studies of the direct effect of thickness on optical transmission are absent to date. In this study, we tackle that theme by discussing the thickness-sensitive optical transmission in VO_2 thin films, with innovative window applications being of special interest. This work shows that dynamic solar control can easily be achieved by varying the geometry of VO_2 films, opening the door to further optical-energy-efficient and adaptable photonic applications.

2. Materials and Methods

A number of methods are employed to produce VO_2 thin films, and each of the methods has its advantages for producing films with desired characteristics. These methods include the sol–gel method,[13] CVD,[14] and atomic layer deposition (ALD).[15,16] The choice of method is critical to determining the resulting material properties of the VO_2 films, such as their optical and electrical properties. Below are the key synthesis techniques and characterization methods employed in this work.

2.1 Fabrication of VO_2 thin films

VO_2 thin films were prepared using a sol–gel technique, depending on the desired film thickness, uniformity, and application requirements. In the sol–gel process, a gel was formed by the hydrolysis and condensation of a vanadium precursor dissolved in isopropanol. This gel was spin-coated onto substrates, dried at 80 °C, and annealed at 500 °C for 1 h. This process produced crystalline VO_2 films with controlled composition and uniformity. Magnetron sputtering was used to improve the surface quality and density of the sol–gel-prepared films. Other common deposition methods for VO_2 thin films include CVD and ALD. In CVD, high-purity VO_2 films with exact stoichiometry and uniform growth over wide areas were produced by vaporizing and reacting vanadium precursors on substrates heated at 450 °C and 1 Torr. ALD allowed for

atomic-scale thickness control of ultrathin films by using alternating pulses of water vapor and vanadium precursor at 200 ℃ for 200 cycles, creating extremely homogeneous films appropriate for applications needing exact optical and electronic tuning. While these methods are well established in the literature, this study is focused exclusively on sol–gel-prepared VO_2 films, some of which were further treated with magnetron sputtering to improve surface quality.

2.2 Choice of substrate

For the deposition of VO_2 thin films, silicon (001) and sapphire (c-plane) substrates were selected because of their lattice structure and chemical stability. Silicon (001) substrates form a native oxide layer that affects the nucleation and growth of the VO_2 film. Sapphire (c-plane) substrates provide a high-temperature ordered lattice with very low defect density, allowing for patterned surfaces and crystalline films. The lattice mismatch that occurs at the VO_2 layer and substrate interface is a major consideration, since it directly affects the continuity and homogeneity of the film, which impacts the final optical and electrical properties. Titanium dioxide (TiO_2) and silica are also widely used substrates for VO_2 deposition, providing environments conducive to film growth without undesirable interactions during deposition. However, silicon and sapphire are considered in this study, as they provide consistency of characterizations and precise comparison of electro-optical characteristics in a constant environment with a high level of reproducibility.

2.3 Film deposition and control of thickness

VO_2 thin films prepared by the sol–gel method were deposited on silicon (001) and sapphire (c-plane) substrates using a magnetron sputtering system under argon atmosphere at 5 mTorr pressure and 200 W power. The thicknesses of the films were 70 and 130 nm, respectively. Sol–gel coating of polydimethylsiloxane (PDMS) substrates was also done, followed by annealing at 450 ℃ to form flexible films with a thickness of 350 nm. Other elastomeric films were, at the same time, used to study both direct and inverse thermal effects. The sputtering and fabrication techniques ensured even deposition and film integrity, which are necessary to ensure that optical and electrical properties remain the same. The film structure and performance were highly influenced by the substrate used. Sapphire substrates were oriented in the c-plane and silicon substrates had a native oxide layer that resulted in discontinuity and no uniformity of the films. Notably, the quality of VO_2 films grown on sapphire was improved because of reduced lattice discrepancy. This shows the relevance of the substrate choice to the structure, optical, and electrical characteristics of VO_2 thin films.

2.4 Characterization techniques

2.4.1 Structural characterization

X-ray diffraction (XRD, JCPDS Card No. 72-0514) and TEM with selected-area electron diffraction (SAED) were employed to determine the crystallographic properties and phase

composition of VO_2 films and nanoparticles. In the case of XRD, the samples were placed on flat holders and subjected to the monochromatic radiation of Cu K (Ka), and the diffraction patterns were recorded as intensity versus 2θ (the angle between the incoming X-ray beam and the detector that measures the diffracted X-rays). Peaks were classified to determine VO_2 phases as monoclinic VO_2 (M) or metastable VO_2 (A). This assisted us in measuring crystallite size, strain effects, and effects of annealing. In the case of TEM analysis, the nanoparticles were dispersed onto copper grids coated with carbon. This enabled the imaging of the particle morphology and size distribution, which ranged between 20 and 50 nm, with high precision. They were also established as having a polycrystalline nature. SAED patterns of specific regions were obtained and, these patterns agreed with the crystallographic patterns obtained in XRD, giving more information of phase and structure.

2.4.2 Surface morphology

SEM (Zeiss LEO 1530) and AFM were used to study the uniformity, roughness, and continuity of VO_2 films. SEM provided high-resolution cross-sectional and top-view images that allowed the observation of multidomain shapes, cracks, and grain boundaries. The characteristics exhibit variation of continuity and density of the magnetron-sputtered, sol–gel-deposited and elastomeric VO_2 films. The roughness of the surface of the VO_2 films was measured by AFM, which enables us to study the structural characteristics at a smaller scale, which is required to establish the importance of surface morphology to the optical and electrical characteristics of the films.

2.4.3 Electrical characterization

A Keithley 2635A source meter with a mounted probe station with a temperature controller was used to measure the temperature-dependent resistivity of VO_2 films. The measurements were performed at the IMT electrode distance of 5 mm. These experiments provided information regarding the effect of substrate-induced lattice mismatch on the IMT. They also affirmed that films that experienced lower lattice strain exhibited superior electrical performance.

2.4.4 Optical characterization

Vibrational modes of the VO_2/*x*NCO films were analyzed at room temperature by Raman spectroscopy (LabRAM ARAMIS, Horiba system). The spectra had characteristic peaks that were associated with the known VO_2 vibrational modes at 140, 192, 223, 260, 308, 338, 387, 395, and 613 cm^{-1}. The lack of peaks corresponding to other vanadium oxides, including V_2O_5, showed high phase purity. The observation of a plateau in the 950–1000 cm^{-1} range indicated that the purity and crystallinity of the VO_2 films were also good, in agreement with past studies. The observation of these Raman measurements before further characterization confirmed the structural integrity of the films.

3. Results and Discussion

3.1 XRD phase composition and peak analysis of VO_2 films

In this study, we employed the XRD method to investigate VO_2 nanoparticles, which were produced by varying the reaction time as 3, 6, and 24 h. This enabled us to determine and analyze the stages of the films produced and how the various process parameters influenced the properties of the materials. The synthesized nanoparticles showed the 'wafer' VO_2 (A) phase, while the VO_2 (M) phase was the preferred mixture. Although the VO_2 (A) phase is monoclinic, it is not very desirable in applications as it is less stable and inferior to the VO_2 (M) phase (rutile phase). The XRD patterns of the 6-h reaction and 24-h reaction showed similar peak intensities. This implies that the increase in reaction time did not have a significant effect on the phase composition with regard to peak intensity. The observed diffraction peaks at 20.87, 33, and 49.84° had overlapping contributions of both VO_2 (A) and VO_2 (M) phases, which means that both phases coexisted in the nanoparticles. Following annealing at 300 °C in vacuum, XRD was used to determine that the structure had changed to the VO_2 (M) phase with the typical diffraction peaks of 27.84, 37.01, 42.19, and 55.56° for the [011], [211], [212], and [−222] planes, respectively. These findings show that the stability and dominance of the VO_2 (M) phase was highly dependent on annealing conditions such as temperature, time, and atmosphere. Since VO_2 is highly oxidized, annealing was performed in vacuum to avoid the creation of other forms of vanadium oxides like V_2O_5, thus ensuring the stability of the rutile phase, which is paramount in obtaining the optical and electrical characteristics desired in applications like smart windows and photonic devices.

The prepared VO_2 thin films were labeled on the basis of their thickness, substrate, and preparation conditions. Sample-Z and Sample-L correspond to VO_2 films deposited on sapphire (c-plane) substrates by magnetron sputtering following the sol–gel process, with thicknesses of 70 nm and 130 nm, respectively. These samples were primarily employed for XRD and TEM analysis.

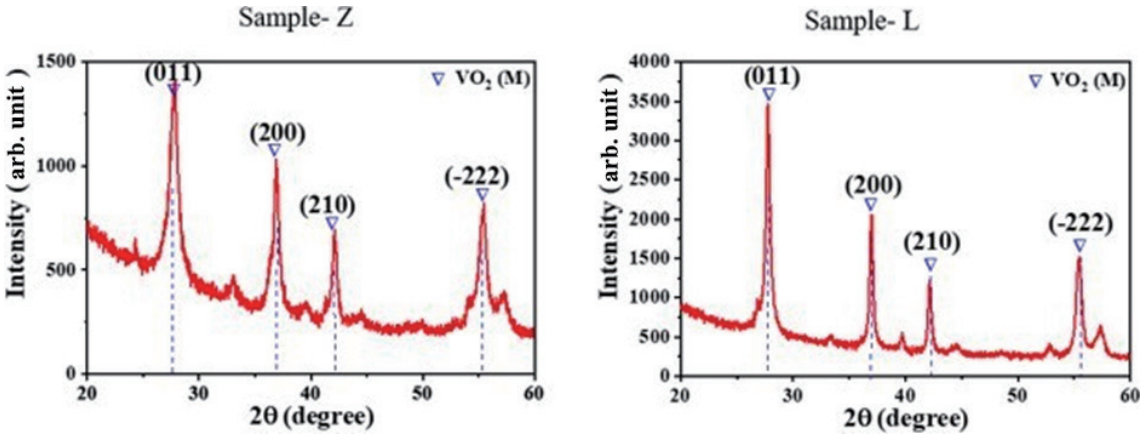

Fig. 1. (Color online) XRD patterns of VO_2 nanoparticles produced with various reaction times.

Reaction time also had a significant effect on peak intensity. Sample 3 displayed XRD peaks of lower intensity than those of the 6- and 24-h samples. This shows that although the VO_2 (M) phase was present, the crystallinity was not as evident, and the transition phase was not complete. By comparison, longer reaction times of 6 to 24 h were beneficial for producing finer crystals and greater uniformity, but the overall composition of the phase was consistent after annealing. In addition to phase composition and crystallinity, other factors influencing the performance of VO_2 films included substrates strain and process-related factors. The mismatch in the lattice between the film and the substrate can alter material properties and affect the phase transition behavior and stability. It is clear from the XRD results that the inclusion of mixed phases is a detrimental feature for a high-quality VO_2 thin film, and successful strategies must be adopted regarding the reaction time and annealing conditions to obtain uniform VO_2 layers. The time spent on synthesis, including operations done through Schlenk line crystallization, was important for creating high-quality films. Together, these factors influence the reliability and functional performance of the films in applications such as smart windows and photonic devices.

3.2 TEM analysis

TEM images were used to confirm the particle sizes and morphologies. Figure 2 shows TEM images of samples synthesized with a 6-h reaction time and annealed at 300 °C for 3 h in low and high resolutions. SAED patterns for the as-synthesized and annealed samples are shown in the insets.

As observed in Fig. 2, the aggregate size of the nanoparticles was between 20 and 50 nm and particles were mostly spherical. The (011) crystal plane exhibited a spacing of 0.32 nm relative to the adjacent crystal plane. Analysis of the SAED patterns and XRD spectra confirmed that the

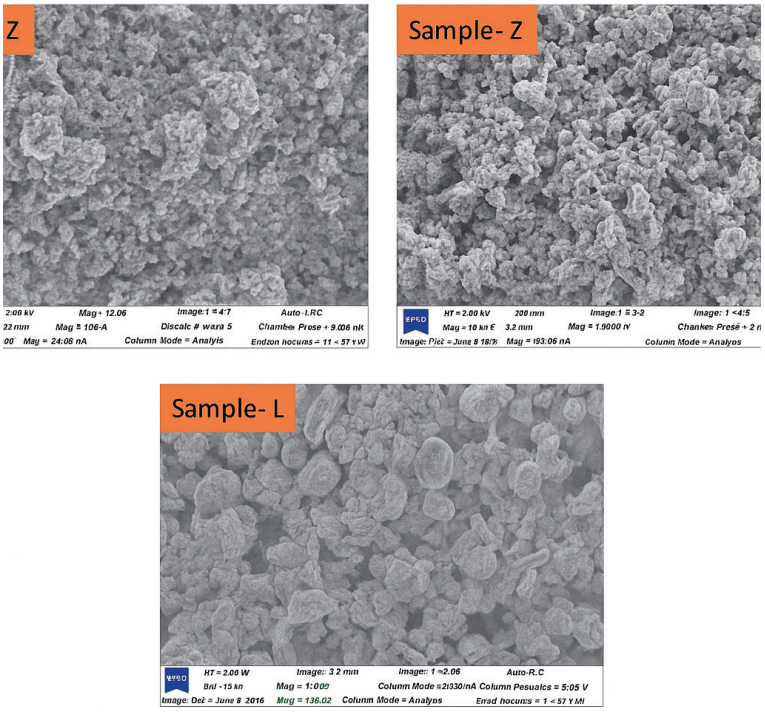

Fig. 2. (Color online) TEM results for sample-Z and -L.

VO_2 (M) nanoparticles had a polycrystalline phase. The d-spacing values determined from the SAED patterns matched the XRD results. Notably, the results of the SAED analysis showed that the as-synthesized VO_2 nanoparticles did not significantly change in size compared with the annealed sample. This supports the idea that structural integrity was maintained during annealing.

Absorption measurements were carried out to determine the optical properties of the VO_2 samples. In the case of the VO_2-ML1 sample, Fig. 3, the highest absorption coefficient was observed at wavelengths between 207 and 232 nm. This is equivalent to a 4.5 eV optical bandgap. The absorption spectra were used to determine the bandgap value with Tauc's relation

$$\alpha h\nu = \left(h\nu - E_g\right)^n. \tag{1}$$

Similarly, the VO_2-ML2 sample, Fig. 4, exhibited a maximum absorption coefficient between 206–240 nm, with an optical bandgap of ~5 eV. The VO_2-NL1 sample, Fig. 5, demonstrated a maximum absorption at 231 nm, corresponding to an optical bandgap of approximately 4.3 eV.

The graph in Fig. 6 shows a decrease in reflectance in the short and long wavelengths. The higher reflectance was at 858 nm with 59% and −11% reflectance for VO_2 ML1 and VO_2 nL1, respectively.

A reduction in reflectance at both shorter and longer wavelengths is shown in Fig. 7. The longer reflectance was at 858 nm with 59% and −11% reflectance for VO_2 ML1 and VO_2 NL1, respectively.

The relationship between absorbance and wavelength was determined using

$$A = -\log\left(\%T\right), \tag{2}$$

where transmission ($\%T$) can be obtained from absorbance using

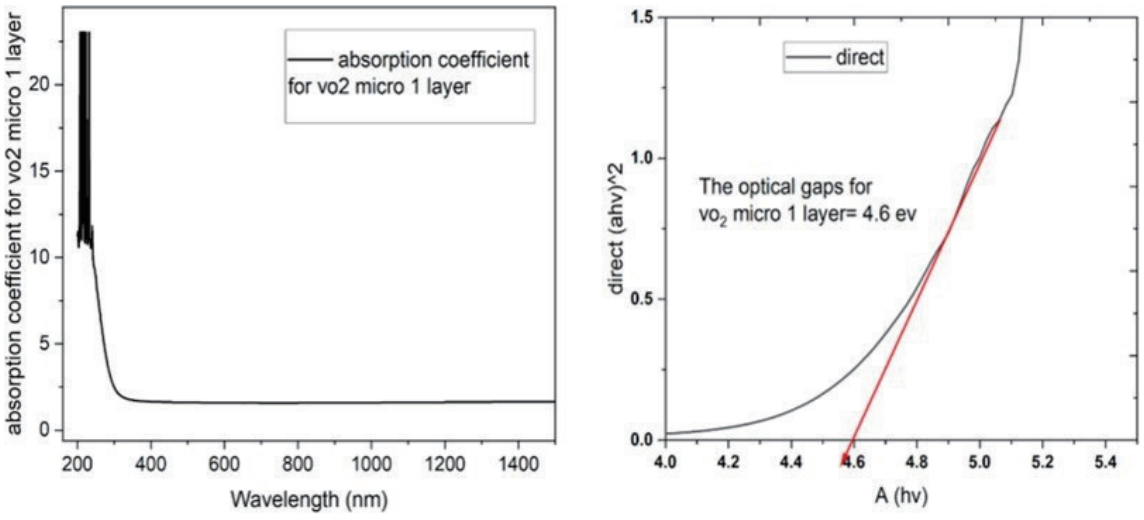

Fig. 3. (Color online) Absorption coefficient and optical bandgap of VO_2-ML1.

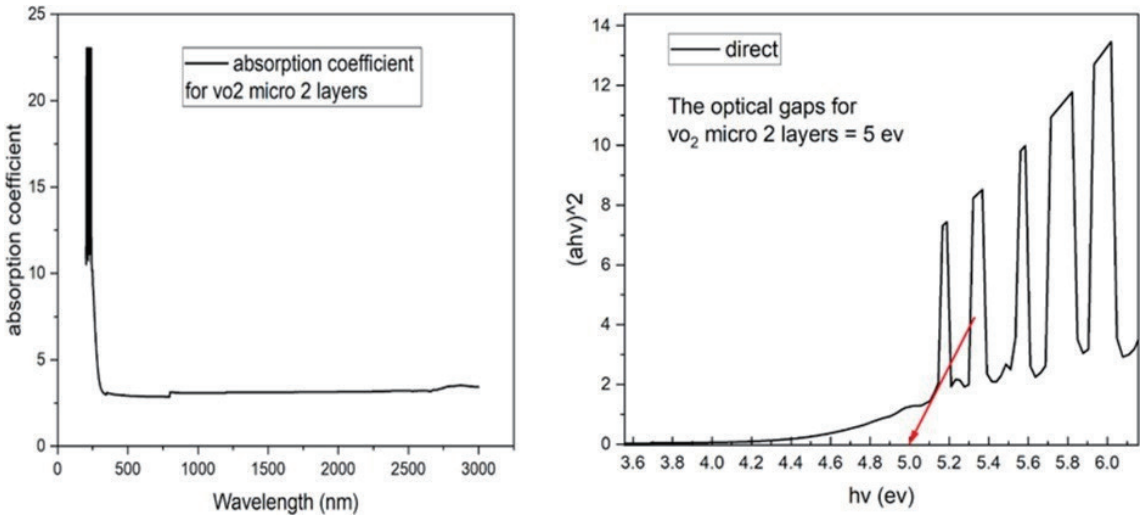

Fig. 4. (Color online) Absorption coefficient and optical gap of VO_2-ML2 (vanadium dioxide).

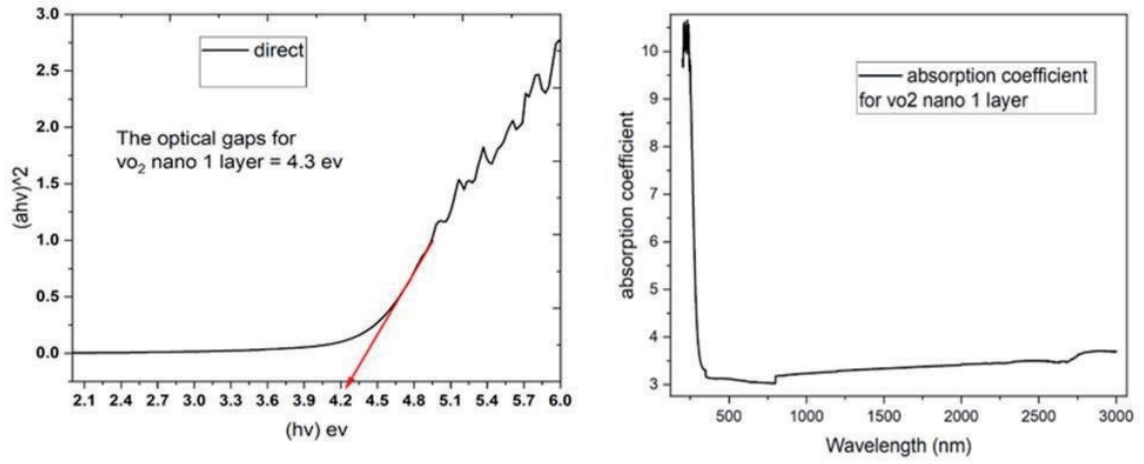

Fig. 5. (Color online) Absorption coefficient and optical bandgap of VO_2-NL1.

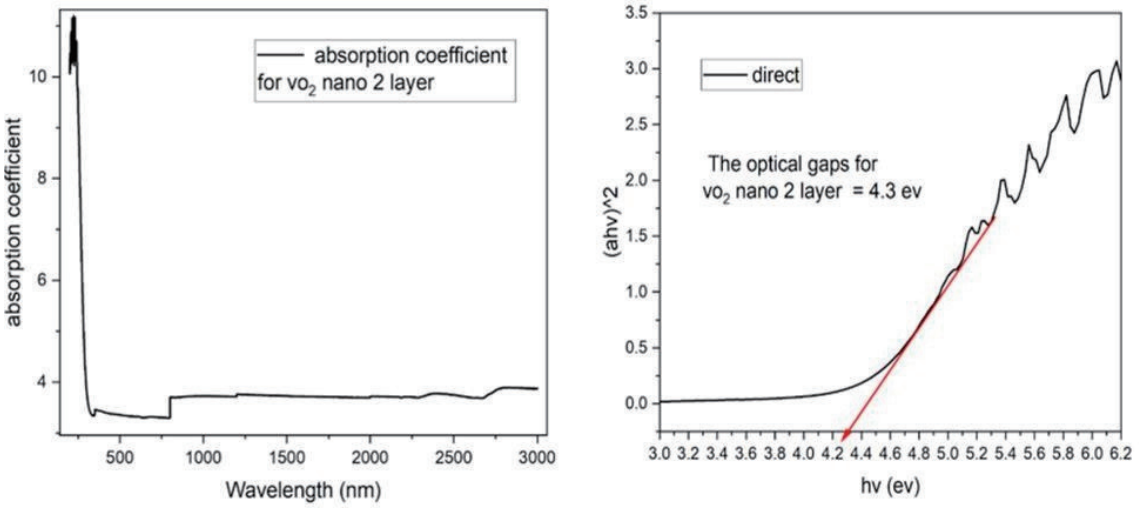

Fig. 6. (Color online) Absorption coefficient and optical bandgap of VO_2-NL2.

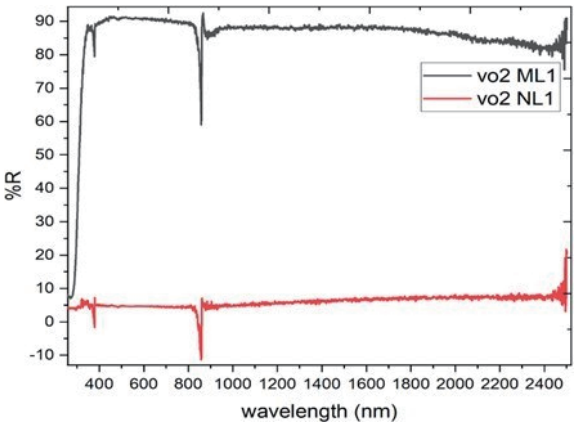

Fig. 7. (Color online) Relationship between reflectance and wavelength.

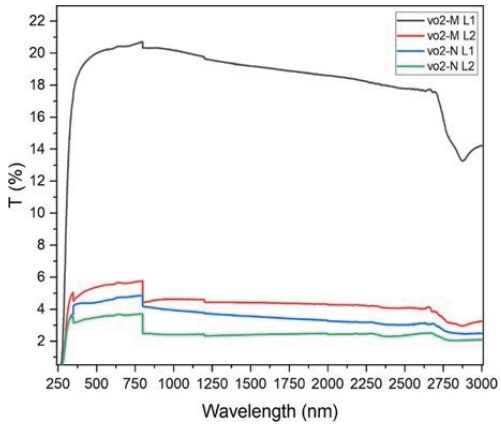

Fig. 8. (Color online) Relationship between transmission and wavelength for all samples.

$$\%T = 10^{-A} \times 100. \tag{3}$$

Figure 8 shows the wavelength-dependent transmission for all samples. The VO_2 ML1 sample exhibited transmission across the 250–1206 nm range, with a maximum transmission of approximately 20% observed at 796 nm.

Structural, morphological, optical, and electrical analyses of sol–gel-prepared VO_2 thin films demonstrate their suitability for thermochromic and photonic applications. XRD and SAED confirmed that annealed films predominantly exhibit the monoclinic VO_2 (M) phase, while as-synthesized nanoparticles showed mixed VO_2 (A) and VO_2 (M) phases, emphasizing the importance of annealing. TEM revealed polycrystalline nanoparticles of 20–50 nm, with (011) plane d-spacing consistent with XRD results, indicating structural integrity. SEM and AFM results showed improved film continuity and uniformity after magnetron sputtering, with sapphire substrates producing higher-quality films due to reduced lattice mismatch. Optical studies revealed thickness-dependent absorption, reflectance, and transmission, with VO_2 ML1 showing ~20% transmission at 796 nm and bandgaps of 4.3–5 eV. Electrical measurements confirmed that lower lattice strain enhances the insulator-to-metal transition, underscoring substrate–film interactions.

4. Conclusions

This paper serves as an introduction to an extensive quantitative research on the optical properties of vanadium dioxide VO_2 nanoparticles with a focus on their possible use in the context of high-tech technologies. Using the optical transmission of different VO_2 thin films, we were able to show that the optical transmittance of the film varies slightly with the thickness of the film, which is useful in understanding the behavior of the material in a variety of setups. This correlation between the thickness and the optical properties is important in improving the performance of VO-based devices. Our results demonstrated that the VO_2 thin film can be

modified to provide better functionality of smart windows, which are dependent on the special semiconductor-to-metal phase change of the material in the control of the solar heat flux. Using the optical characteristics of VO_2, which are dependent on the phase of operation, these smart windows will be able to adjust temperatures automatically, which will help to save energy in buildings and lower the need to use standard heating and air-conditioning equipment. The results of this study highlight the need and significance of further enhancement and improvement of VO_2 thin films to realize their full potential in practical applications, which will lead to a wider use of energy-efficient technology and adaptive optical systems. Further studies must be carried out in the future to incorporate these materials in scalable production processes so that they can be easily transferred to commercial use.

Declaration of competing interest

The authors declare that they have no known competing financial interests or personal relationships that could have appeared to influence the work reported in this paper.

Funding

This research work was supported by King Abdul-Aziz University, DSR, Jeddah, Saudi Arabia under grant no. (IPP 201-665-2025). Therefore, the author gratefully acknowledges the technical and financial support from the Ministry of Education, King Abdul-Aziz University, DSR, Jeddah, Saudi Arabia.

Data Availability Statement

No primary data was used for the research described in the article.

Acknowledgments

The authors gratefully acknowledge technical support from the Ministry of Education, King Abdul-Aziz University, DSR, Jeddah, Saudi Arabia.

Ethical statement

Not applicable.

References

1 C. N. Berglund and H. J. Guggenheim: Phys. Rev. **185** (1969) 1022. https://doi.org/10.1103/PhysRev.185.1022
2 Y. Zhang, W. Xiong, W. Chen, and Y. Zheng: Nanomaterials **11** (2021) 338. https://doi.org/10.3390/nano11020338
3 X. Huang, W. Yang, and U. Eckern: Unpublished preprint (1998).

4 A. Rashidi, S. R. Entezar, and A. Hatef: Nanotechnology **31** (2020) 335701. https://doi.org/10.1088/1361-6528/ab8e9c
5 G. H. Liu, X. Y. Deng, and R. Wen: J. Mater. Sci. **45** (2010) 3270. https://doi.org/10.1007/s10853-010-4306-1
6 E. Strelcov, A. V. Davydov, U. Lanke, C. Watts, and A. Kolmakov: ACS Nano **5** (2011) 3373. https://doi.org/10.1021/nn2007089
7 T. Chang, Y. Zhu, C. Cao, C. Yang, H. Luo, P. Jin, and X. Cao: Acc. Mater. Res. **2** (2021) 714. https://doi.org/10.1021/accountsmr.1c00044
8 I. G. Madida, A. Simo, B. Sone, A. Maity, J. B. Kana Kana, A. Gibaud, G. Merad, F. T. Thema, and M. Maaza: Sol. Energy **107** (2014) 758. https://doi.org/10.1016/j.solener.2014.06.025
9 S. Majid, K. Gautam, and A. Ahad, *et al*.: Unpublished preprint (2019).
10 V. V. Strelchuk, O. F. Kolomys, D. M. Maziar, V. P. Melnik, B. M. Romanyuk, O. Y. Gudymenko, O. V. Dubikovskyi, and O. I. Liubchenko: Mater. Sci. Semicond. Process. **174** (2024) 108224. https://doi.org/10.1016/j.mssp.2024.108224
11 J. Sun and G. K. Pribil: Appl. Surf. Sci. **421** (2017) 819. https://doi.org/10.1016/j.apsusc.2017.05.174
12 I. Derkaoui, M. Khenfouch, M. Benkhali, and A. Rezzouk: J. Phys.: Conf. Ser. **1292** (2019) 012010. https://doi.org/10.1088/1742-6596/1292/1/012010
13 G. Pan, J. Yin, K. Ji, X. Li, X. Cheng, H. Jin, and J. Liu: Sci. Rep. **7** (2017) 6132. https://doi.org/10.1038/s41598-017-05229-9
14 B. Rajeswaran and A. M. Umarji: Mater. Chem. Phys. **245** (2020) 122230. https://doi.org/10.1016/j.matchemphys.2020.122230
15 A. P. Peter, K. Martens, G. Rampelberg, M. Toeller, J. M. Ablett, J. Meersschaut, D. Cuypers, A. Franquet, C. Detavernier, J.-P. Rueff, M. Schaekers, S. Van Elshocht, M. Jurczak, C. Adelmann, and I. P. Radu: Adv. Funct. Mater. **25** (2015) 679. https://doi.org/10.1002/adfm.201402687
16 M. Nishikawa, T. Nakajima, T. Manabe, T. Okutani, and T. Tsuchiya: J. Ceram. Soc. Jpn. **118** (2010) 788. https://doi.org/10.2109/jcersj2.118.788